Advances in first-principles modelling of point defects in UO_2: f electron correlations and the issue of local energy minima

2013 J. Phys.: Condens. Matter 25 333201

(http://iopscience.iop.org/0953-8984/25/33/333201)

IOP PUBLISHING JOURNAL OF PHYSICS: CONDENSED MATTER
J. Phys.: Condens. Matter **25** (2013) 333201 (13pp) doi:10.1088/0953-8984/25/33/333201

TOPICAL REVIEW

Advances in first-principles modelling of point defects in UO_2: f electron correlations and the issue of local energy minima

B Dorado[1], M Freyss[2], B Amadon[1], M Bertolus[2], G Jomard[2] and P Garcia[2]

[1] CEA, DAM, DIF, F-91297 Arpajon, France
[2] CEA, DEN, DEC, Centre de Cadarache, F-13108, Saint-Paul-Lez-Durance, France

E-mail: boris.dorado@cea.fr

Received 25 March 2013, in final form 21 June 2013
Published 29 July 2013
Online at stacks.iop.org/JPhysCM/25/333201

Abstract
Over the last decade, a significant amount of work has been devoted to point defect behaviour in UO_2 using approximations beyond density functional theory (DFT), in particular DFT + U and hybrid functionals for correlated electrons. We review the results of these studies from calculations of bulk UO_2 properties to the more recent determination of activation energies for self-diffusion in UO_2, as well as a comparison with their experimental counterparts. We also discuss the efficiency of the three known methods developed to circumvent the presence of metastable states, namely occupation matrix control, U-ramping and quasi-annealing.

(Some figures may appear in colour only in the online journal)

Contents

1. Introduction

Uranium dioxide UO_2 is the standard nuclear fuel used in pressurized water reactors. During in-reactor operation, the fission of uranium atoms produces a wide variety of fission products that create point defects as they deposit their energy in the surrounding material, which in turn governs the fuel microstructure evolution. Most of the fission products that are created are short-lived isotopes and those with half-lives of over a few days have a significant impact on the behaviour of UO_2 under irradiation. They have a direct influence on the oxide thermal conductivity (hence temperature), cladding corrosion during fuel–cladding mechanical interaction and interaction with the coolant in the case of cladding failure. It is therefore very important to understand how point defects and fission products behave in UO_2 in order to gain insight into fuel evolution under irradiation.

First-principles modelling, based on density functional theory (DFT) [1, 2], is the basis of multiscale approaches. It gives access to relevant and important information that can be used as input data for higher-scale models. Moreover, coupling first-principles modelling with experiments allows one to gain insight into fundamental properties and/or mechanisms that are not available through experiment alone and that govern the behaviour of point defects and fission products.

First-principles studies of the behaviour of UO_2 under irradiation began in the late 1990s. Petit *et al* [3] first studied point defects in the local density approximation (LDA) of the DFT, using the linear muffin-tin orbital (LMTO) formalism. They then studied for the first time the stability of krypton in the oxide [4]. Crocombette *et al* [5, 6] later studied the stability in UO_2 of point defects and a number of fission products (including krypton, iodine, and xenon) using plane waves and pseudopotentials. Using the generalized gradient approximation (GGA), Freyss *et al* [7, 8] studied point defects, as well as helium and xenon stability in UO_2, which constituted an improvement over LDA calculations.

All the above studies have generated the first *ab initio* formation and incorporation energies of point defects and fission products. UO_2, however, exhibits strong f electron correlations and is a Mott insulator. Neither the LDA nor the GGA is able to entirely capture these correlation effects. As a consequence, the electronic structure of UO_2 is not well described with these approximations. In order to improve the modelling of UO_2, other approximations beyond DFT should be used. The present review is dedicated to the studies that have been carried out on perfect and defective UO_2 using approximations beyond DFT, with a focus on the most widely used DFT + U (LDA + U and GGA + U) approximation. Note that the stability of fission products in UO_2 will not be covered here since it has already been reviewed by Liu *et al* [9]. Particular care will be taken to compare results from all the various studies and to point out any discrepancy, most of which can be ascribed to the presence of metastable states (see section 3).

The review is organized as follows: section 2 describes the approximations beyond standard DFT that have been developed to describe strongly correlated materials like UO_2. Section 3 introduces the issue of local energy minima that arises when the above approximations are used. The three known methods to circumvent the difficulties associated with these metastable states are presented. In section 4 we review some experimental studies of interest that were carried out on UO_2 in order to determine ground state properties, as well as point defect behaviour. The DFT results presented in section 5 are then compared with their experimental counterparts as an assessment of approximations beyond DFT, and in particular of the methods aimed at tackling the issue of the metastable states.

2. The DFT + U approximation for strong electron correlations

As mentioned in the Introduction, standard approximations of the DFT (namely the LDA and GGA), although efficient, fail to capture entirely strong electron correlations that arise in materials like UO_2. This results in the electronic structure of UO_2 not being correctly described. With LDA and GGA, UO_2 is predicted to be a metal instead of an insulator. Several approximations have been specially developed to improve this shortcoming. They are the hybrid functionals [10–12], the self-interaction correction (SIC) [13] and approximations based on the addition of a Hubbard term to the Hamiltonian, namely the DFT + U [14–16] and the dynamical mean field theory (DFT + DMFT) [17, 18]. In this review we will focus on the DFT + U approximation since it is the most widely used approximation for studying the behaviour of point defects and fission products in nuclear fuels. Indeed, in such studies, supercells of up to a hundred atoms have to be used, which has until now forbidden the use of all other approximations due to prohibitive computational cost. Extensive details of other approximations beyond DFT can be found in the corresponding references. We should also point out the existence of another type of hybrid functional, called 'exact exchange for correlated electrons' (EECE) [19], which applies the exact exchange to a restricted subspace formed by the correlated electrons of a correlated system. This hybrid functional approach yields satisfying results and is less computationally demanding than the original one. It is therefore used in several studies of point defect behaviour in UO_2.

In the DFT + U approximation, a correction is added to the LDA and GGA functionals that describes the enhanced interactions between correlated electrons. The DFT + U functional is given by

$$E_{\mathrm{DFT+U}} = E_{\mathrm{DFT}} + E_{\mathrm{Hub}} - E_{\mathrm{dc}}, \tag{1}$$

where E_{DFT} is the contribution of the LDA/GGA to the total energy, E_{Hub} is the correction that takes into account the interaction between correlated electrons and E_{dc} is the double counting term aimed at removing the LDA/GGA contribution to this interaction. The two most widely used expressions for the Hubbard term have been introduced by Liechtenstein [15] and Dudarev [16], the latter being a simplified version of the former. Irrespective of the approach used, and in a diagonal basis for correlated occupation matrices, E_{Hub} can be written as [14, 20]

$$E_{\mathrm{Hub}} = \tfrac{1}{2} \sum_{m\sigma \neq m'\sigma'} W^{\sigma\sigma'}_{mm'} n^{\sigma}_{m} n^{\sigma'}_{m'}, \tag{2}$$

where n^{σ}_{m} is the number of electrons on the orbital (m, σ) and $W^{\sigma\sigma'}_{mm'}$ is a matrix element for the Coulombic interaction. $W^{\sigma\sigma'}_{mm'}$ represents the interaction between an electron with spin σ on the orbital m and another electron with spin σ' on the orbital m'. $W^{\sigma\sigma'}_{mm'}$ can be expressed in terms of the direct and exchange integrals:

$$W^{\sigma\sigma'}_{mm'} = (U_{mm'} - J_{mm'}\delta_{\sigma\sigma'}). \tag{3}$$

Diagonal terms in the W matrix are not taken into account in (2), therefore there is no self-interaction in the Hubbard term. As for the double counting term, it can be expressed either in the around-mean field (AMF) or the

fully-localized limit (FLL) approach, both introduced by Czyżyk and Sawatzky [21]. All studies of UO_2 published so far use the FLL double counting term, which is written as

$$E_{\mathrm{dc}}^{\mathrm{FLL}} = \tfrac{1}{2}UN(N-1) - \tfrac{1}{2}J\sum_{\sigma}\left(N_{\sigma}^{2} - N_{\sigma}\right). \qquad (4)$$

In (4), N is the total number of electrons and N_σ is the total number of electrons with spin σ. It should also be noted that another DFT + U approach has been developed by Zhou *et al* [22]. It is a self-interaction free form of the original DFT + U that enables restoration of the degeneracies of the atomic orbitals in the free ion, resulting in the correct ground state for atomic species.

Finally, the value of U is expected to depend on the local environment, the point group symmetry and the charge state of the ion it is applied to. This in turn means that accurate calculations with DFT + U should in principle include a self-consistent determination of U for each inequivalent ion in the simulation cell, using for instance constrained LDA [23], linear response theory [24] or constrained random-phase approximation [25, 26]. For UO_2, the U and J values were estimated by Yamazaki and Kotani [27, 28] based on an analysis of x-ray photoemission spectra, who found $U = 4.50$ eV and $J = 0.54$ eV. The U value was also calculated from first principles by Yin *et al* [29] using a many-body GW approach. They found $U = 6$ eV, which is significantly larger than the value estimated by Yamazaki and Kotani.

3. The problem of metastable states

3.1. Origin of metastable states

With LDA or GGA, correlated orbitals in UO_2 have roughly the same energy. This results in fractional occupancies of the f orbitals, and hence a metallic character. On the contrary, the DFT + U approximation localizes electrons on specific orbitals, leading to an insulating character. The price to pay for this localization in DFT + U is the occurrence of metastable states [30–33] that correspond to the various ways of filling the orbitals: in UO_2, the metastable states correspond to the filling of the seven 5f orbitals by the two 5f electrons of the U^{4+} ions.

The number of metastable states is directly related to the orbital degeneracies. In paramagnetic UO_2, the point group symmetry of the uranium site is O_h and the crystal field lifts the seven 5f orbital degeneracies into a 3–1–3 configuration (sorted by increasing energy). The introduction of antiferromagnetic order then changes the point group symmetry of the uranium site to D_{4h}, which in turn lifts the degeneracies into a 2–1–1–2–1 configuration. Finally, the Jahn–Teller distortion that occurs below the Néel temperature (see section 4.1.2) further lifts all degeneracies into a 1–1–1–1–1–1–1 configuration. Figure 1 shows a schematic of the splitting of the 5f orbitals depending on the point group symmetry of the uranium site. Since orbital degeneracies constrain the electronic occupancies, it reduces the number of metastable states but makes the ground state harder to reach [34–36].

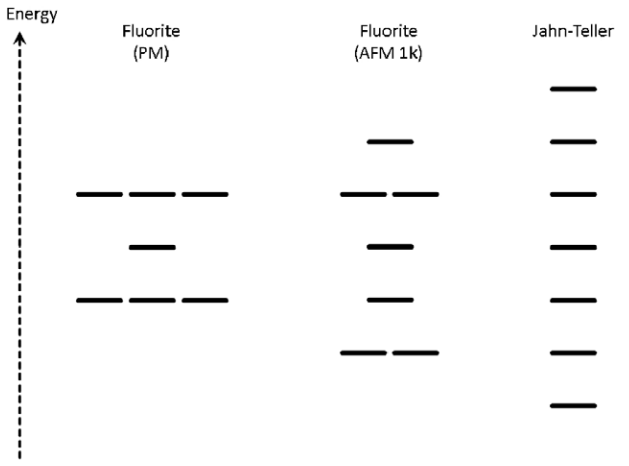

Figure 1. Splitting of the uranium 5f orbitals in UO_2 depending on the point group symmetry of the uranium site, calculated in the LDA.

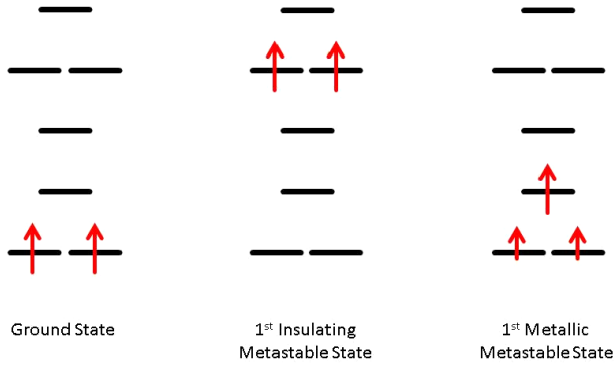

Figure 2. Electronic occupancies of the ground state, the first metastable state and the first metallic state of UO_2 with the 1***k*** antiferromagnetic order and the LDA energy levels.

From the study of the ground state and metastable states in UO_2 (1***k*** antiferromagnetic order) [34], we can infer that the ground state is obtained by putting the two 5f electrons in the two lowest two-fold degenerate orbitals, whereas the first metastable state is obtained by filling the two higher two-fold degenerate orbitals. Figure 2 shows the corresponding electronic occupancies, as well as those of the first metallic state. It may appear surprising that the first metastable state (located only 12 meV/UO_2 above the ground state) is obtained by putting the two electrons on such high energy orbitals. This is because the DFT + U formalism favours integer occupancies by applying an energy penalty to fractional occupancies. Therefore, orbitals that are filled with an integer number of electrons will end up lower in energy than those filled with a fractional number of electrons. Note that because the first metastable state lies only 12 meV/UO_2 above the ground state, fluctuations between different states are possible at finite temperature, which is an effect that is not described by static mean field methods, such as DFT + U. In order to account for fluctuations between electronic states (hence occupancies), one can use the DFT + DMFT with the Hubbard I approximation, as has been done in [37].

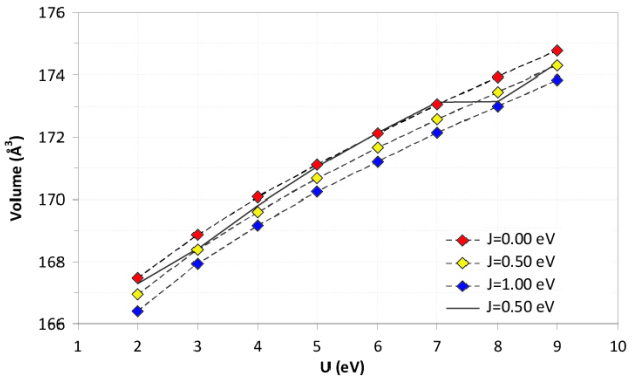

Figure 3. Variation of the 12-atom UO_2 cell volume as a function of the U and J parameters of the Liechtenstein DFT + U [34]. The black curve corresponds to calculations with random initial occupancies while the coloured curves include a proper treatment of the metastable state problem (here, the occupation matrix control scheme).

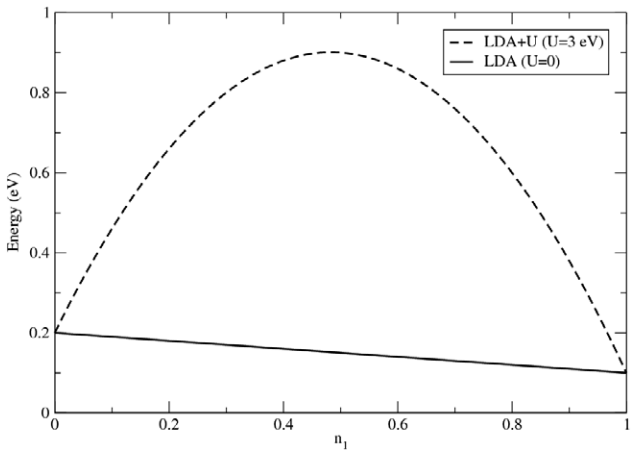

Figure 4. Total energy of a one-electron system with two states available for the electron ($\epsilon_1 = 0.1$ eV and $\epsilon_2 = 0.2$ eV). The full and dotted lines represent the LDA and LDA + U calculations, respectively.

The occurrence of metastable states is not a new topic. Indeed the Hartree–Fock approximation, which constitutes the basis of the DFT + U method, has been known since the 1960s to yield multiple energy minima [38, 39]. In practical calculations, this implies that a calculation starting with random initial occupancies calculated from random initial wavefunctions won't necessarily converge to the ground state. On more complex systems, such as defective UO_2 supercells, consecutive runs of the same calculation will yield total energies that are significantly different. A simple indication of the presence of metastable states can be seen in figure 3 [34], which shows the variation of the volume of a 12-atom conventional cell as a function of the U parameter of the DFT + U. We clearly see that out of a series of calculations starting with slightly different cell parameters, some will reach the ground state while others will reach metastable states, which exhibit different volumes. On the contrary, the curves that are obtained using a proper treatment for metastable states are smooth and do not display any 'jump' from one state to another.

The problem lies in the fact that once the calculation has reached a metastable state, it remains irreversibly trapped in that state. To illustrate that, let us consider the simplest DFT + U energy functional describing a one-electron system with two possible states for the electron (with energies ϵ_1 and ϵ_2, respectively). The ground state has the energy ϵ_1. The energy functional can be written as

$$E(n_1, n_2) = \epsilon_1 n_1 + \epsilon_2 n_2 + U n_1 n_2, \tag{5}$$

where n_1 and n_2 are the occupation numbers of the two states with energies ϵ_1 and ϵ_2, respectively, and U is the interaction term (namely, the DFT + U correction) between the two states. Since $n_1 + n_2 = 1$, (5) can be rewritten as

$$E(n_1) = \epsilon_1 n_1 + \epsilon_2 (1 - n_1) + U n_1 (1 - n_1). \tag{6}$$

Figure 4 shows the corresponding plot in the LDA ($U = 0$) and LDA + U ($U = 3$ eV), with $\epsilon_1 = 0.1$ eV and $\epsilon_2 = 0.2$ eV. We see that in the LDA calculation, if the electron is in the metastable state with energy ϵ_2 it will be able to easily reach the ground state, with energy ϵ_1. On the contrary, in the LDA + U calculation, because of the additional interaction term, there is an energy barrier to cross in order to reach the ground state. As a result, once the electron is stuck in a metastable state, it would require too large an energy to reach the ground state, unless additional help is provided by the user via one of the methods described in section 3.2.

3.2. Methods developed to circumvent the problem

In order to perform accurate DFT + U calculations and make sure that they converge to the ground state of the system, an ad hoc procedure has to be applied to avoid the convergence of the calculations to a local energy minimum. To this date three methods have been developed: occupation matrix control, quasi-annealing and U-ramping. We recall below their basic features:

- The occupation matrix control (OMC) [34, 40, 41] scheme uses occupation matrices (which represent how the correlated electrons occupy the correlated orbitals) to precondition the convergence of the system towards the ground state. The ground state must first be found by imposing all possible initial occupation matrices (hence all possible initial electronic occupancies) and by comparing the corresponding total energies, the lowest being that of the ground state. Once the ground state is found, the associated electronic configuration is imposed at the beginning of all subsequent calculations in order to ensure the calculation does not 'jump' out of the ground state configuration.
- The quasi-annealing scheme (QA) [42] involves a fictitious fluctuation of the external potential, which is gradually suppressed in order to explore the potential energy surface.
- The U-ramping scheme [43] requires a gradual increase in the U parameter of the DFT + U from 0 (standard

Table 1. Bulk modulus B and elastic constants of UO_2 determined from experiments in the fluorite phase.

	Wachtman 1965 [49]	Marlow 1969 [50]	Fritz 1976 [51]	Benedict 1982 [52]	Idiri 2004 [47]
B (GPa)	213	203	209	190	207
C_{11} (GPa)	396		389		
C_{12} (GPa)	121		119		
C_{44} (GPa)	64		60		

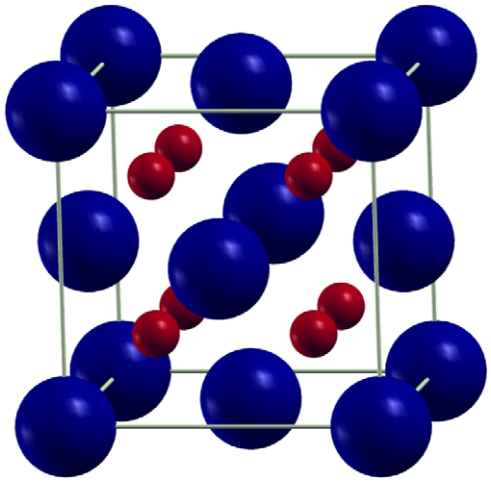

Figure 5. Fluorite structure of UO_2 from the perspective of the uranium sublattice. Dark blue and red spheres stand for uranium and oxygen atoms, respectively.

DFT calculation) to its desired value, typically by steps of 0.1 eV. This method assumes that orbital ordering is unchanged between DFT and DFT + U.

It is also worth noticing that a method based on metadynamics [44], which has yet to be applied with DFT + U, has been developed and therefore constitutes an interesting alternative to the three methods described above. Finally, the existence of metastable states and the breaking of symmetry is a drawback of any static mean field theory, and could be partially overcome by DFT + DMFT [37, 45], but at a much greater computational cost.

4. Experimental studies

4.1. Fluorite and Jahn–Teller phases of UO_2

4.1.1. The fluorite phase. Above the Néel temperature (T_N = 30.8 K), UO_2 crystallizes in the fluorite structure, as determined for the first time in 1963 using neutron diffraction [46]. In the fluorite structure, uranium atoms form a face centred cubic lattice with oxygen atoms located in the tetrahedral sites (figure 5). From the oxygen perspective, the fluorite structure can be seen as a cubic lattice with oxygen atoms located on the cube vertices and uranium atoms at the centre of every other cube. The fluorite space group is $Fm\bar{3}m$ and the point group symmetry of the uranium site is O_h.

The cell parameter of the fluorite phase is 5.47 Å [47]. The bulk modulus B and elastic constants C_{11}, C_{12} and C_{44} have been reported in the literature and are shown in table 1. The bulk modulus is approximately 200 GPa and the most recent value is 207 GPa. The temperature dependence of the elastic constants has been measured by Brandt and Walker [48]. They showed the existence of a first-order transition in the variation of the elastic constants at T_N, except for C_{44} which is strongly reduced below 200 K because of the phase transition that occurs at the Néel temperature.

The first electronic structure measurements in UO_2 were carried out in 1980 by Baer and Schoenes [53] using x-ray photoemission spectroscopy (XPS) and bremsstrahlung isochromate spectroscopy (BIS). The measured XPS spectra were later analysed by Yamazaki and Kotani [27, 28] via the Anderson impurity model in order to estimate the values of the Coulomb and exchange energies for uranium 5f electrons in UO_2, as discussed above. The determination of the electronic structure of UO_2 has also provided us with a bandgap value of around 2 eV [53–55], as well as a cohesive energy of 21.9 eV [56].

From a magnetic standpoint, the fluorite structure of UO_2 is a Curie–Weiss type paramagnet [57, 58]. Using inelastic neutron diffraction, Caciuffo *et al* [59] showed the existence of a Jahn–Teller (JT) distortion in the fluorite phase that affects the oxygen sublattice, with oxygen ions moving in the ⟨100⟩ direction (1$\boldsymbol{k}$ distortion). The distortion is dynamical and continually fluctuating, yielding on average a fluorite structure. When the temperature reaches the Néel temperature, the dynamical distortion turns into a static JT distortion that is responsible for the electronic and magnetic properties of UO_2 at low temperature.

4.1.2. The Jahn–Teller phase. The structure of the JT phase of UO_2 is not as documented as that of the fluorite phase. It is known that the oxygen ions move approximately 0.014 Å away from their fluorite positions in the ⟨111⟩ directions (3$\boldsymbol{k}$ distortion) [58]. Moreover, the Brandt and Walker study [48] provides us with the temperature dependence of the elastic constants. By extrapolation, we can have an estimate of the elastic constants at 0 K: C_{11} = 400 GPa, C_{12} = 126 GPa, and C_{44} = 59 GPa. Therefore, at 0 K, the elastic constants of the JT phase are similar to those of the fluorite phase at ambient temperature (displayed in table 1).

Unlike the structural and mechanical properties, the electronic and magnetic properties of the JT phase have been widely reported. The phase transition at 30.8 K was first observed by Jones *et al* [60] using specific heat measurements. According to the magnetic susceptibility behaviour at high temperature, they stated an AFM ordering,

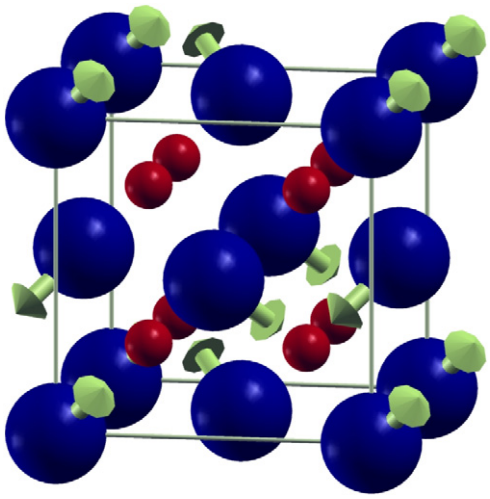

Figure 6. Jahn–Teller phase of UO_2 with a noncollinear 3***k*** antiferromagnetic order. Dark blue and red spheres stand for uranium and oxygen atoms, respectively. The arrows represent the directions of the magnetic moments of the uranium atoms.

which was confirmed a few years later by Arrott and Goldman [61]: below 30.8 K, UO_2 is AFM, with a magnetic moment of 1.74(2) μ_B/uranium atom [62, 63]. Even though the AFM character of the JT phase has been known since the 1950s, the exact nature of the AFM order was determined only recently. Allen [64, 65] first suggested a 1***k*** AFM order, with collinear magnetic moments in the ⟨100⟩ directions. Subsequent neutron diffraction studies [63, 66] confirmed the JT distortion but suggested a 2***k*** AFM order, with magnetic moments in the ⟨110⟩ directions. A 3***k*** AFM order was finally proposed by Burlet *et al* [67] in order to account for the results they obtained using neutron diffraction under a magnetic field. Indirect measurements were later reported in the literature [68, 69] and the 3***k*** AFM order could be observed directly only recently using resonant x-ray diffraction [70]. Figure 6 shows the JT phase of UO_2.

4.2. Oxygen and uranium self-diffusion

Activation energies for self-diffusion can be compared to DFT-based calculations via a point defect model (see section 5.2.3). They have been reported in the literature for both oxygen [71–75] and uranium [73, 76–79] self-diffusion.

For oxygen self-diffusion, previous determinations of the activation energy provided us with a value of about 2.5 eV [71–75]. It was pointed out, however, that these studies did not involve careful control of all the relevant physical parameters such as equilibrium oxygen partial pressure, impurity content and temperature. New experiments [75, 80] were later carried out under controlled oxygen partial pressure, temperature and impurity content. They provided an activation energy of 0.75 ± 0.08 eV, which is significantly different from previous estimates.

As for uranium self-diffusion, previous experimental results suffer from the same difficulties outlined above for oxygen diffusion. An additional cause of scatter is the enhanced diffusion at the grain boundaries, with a diffusion coefficient that is five orders of magnitude greater than the volume diffusion coefficient, between 1773 and 1973 K in a reducing atmosphere [81]. Activation energies for uranium self-diffusion have been reported for near stoichiometric and stoichiometric UO_2 single crystals ranging from 4.4 eV to 5.6 eV [73, 76–79]. To date, however, no new experiments have been carried out, contrary to the case for oxygen diffusion.

5. DFT-based studies

5.1. UO_2 bulk properties

5.1.1. Finding the ground state. Before going through the calculated physical properties of perfect UO_2, we briefly outline the attempts made to find the ground state of UO_2 with approximations beyond DFT. It is difficult to compare the results obtained by authors who used the methods described in section 3.2 because the states reached are strongly dependent upon the calculation details. In fact, a direct comparison of calculations performed using different parameters is impossible. The only way one can perform a comparison is to have access to the occupation matrices of all the different studies and compare the total energies obtained using OMC, which is currently the only method that has direct control over occupation matrices. Unfortunately occupation matrices are usually not provided.

In addition, the first study of the ground state and metastable states of UO_2 [34] showed that one of the most important parameters for finding the ground state is the breaking of symmetries. This had already been pointed out by Larson *et al* [33] in their study on rare earth nitrides. Indeed, symmetries induce orbital degeneracies that constrain the search for the ground state.

Finally, another important point is that in almost all DFT-based studies, UO_2 was modelled using a 1***k*** AFM order (see figure 7), which is the simplest magnetic ordering that allows one to correctly reproduce the bandgap and the structural properties of UO_2. Recently, however, paramagnetic (PM) UO_2 could be described with DFT + U by considering it as an alloy of spin up and spin down components [82], therefore allowing the use of small supercells (24 atoms) with collinear magnetic moments.

For all the above reasons, and in order to avoid any confusion, we will therefore from now on clearly indicate the magnetic order considered in each study, as well as whether or not symmetries have been kept in the calculations, as it can strongly affect the interpretation of the results.

Dorado *et al* [34, 36] performed a systematic search of the ground state of crystalline 1***k*** AFM UO_2 with symmetries, both in the Liechtenstein and Dudarev approach of the DFT + U. They provided the corresponding ground state occupation matrices expressed in the basis of real spherical harmonics. They also showed that with symmetries the Dudarev ground state is the Liechtenstein first metastable state, and vice versa [36]. The latter result underlines that these two states are nearly degenerate, hence the need for a

Table 2. UO_2 bulk properties (cell parameters, cohesive energy E_{coh}, bulk modulus B, and bandgap Δ), calculated with different approximations beyond DFT, including DFT + U with different functionals, hybrid functionals (PBE0, HSE, EECE), and SIC.

Authors	Approx.	Basis	(a, b, c) (Å)	E_{coh} (eV)	B (GPa)	Δ (eV)
Dudarev [84]	LSDA + U	LMTO/ASA	(5.36, 5.36, 5.36)			1.1
Dudarev [85]	LSDA + U	LMTO/ASA	(5.37, 5.37, 5.37)	22.2	173	1.3
Yun [86]	PBE + U	PAW	(5.44, 5.44, 5.44)	20.3	209	1.8
Iwasawa [87]	PBE + U	PAW	(5.52, 5.52, 5.47)		190	1.8
Prodan [32]	PBE0	GAUSSIANS	(5.45, 5.45, 5.45)		219	3.1
	HSE		(5.46, 5.46, 5.46)		222	2.4
Gupta [88]	PW91 + U	PAW	(5.52, 5.52, 5.52)	21.7	209	1.8
Geng [89]	LSDA + U	PAW	(5.44, 5.44, 5.44)	32.8	208	1.5
	PBE + U		(5.55, 5.55, 5.55)	28.8	181	1.6
Nerikar [90]	PW91 + U	PAW	(5.49, 5.49, 5.49)			1.9
Gryaznov [91]	LSDA + U	PAW	(5.46, 5.46, 5.42)	26.0	196	1.8
	PBE + U		(5.57, 5.57, 5.51)	23.0	180	1.9
	PW91 + U		(5.56, 5.56, 5.51)	23.1	183	1.9
Yu [92]	GGA + U	PAW	(5.54, 5.54, 5.49)	21.2		1.2
Dorado [34]	PBE + U	PAW	(5.57, 5.57, 5.49)		187	2.3
Jollet [35]	EECE	PAW	(5.51, 5.51, 5.51)		199	2.0
Petit [93]	SIC	LMTO/ASA	(5.47, 5.47, 5.47)		219	2.6
Devey [94]	GGA + U	PAW	(5.54, 5.54, 5.54)		197	2.6
Sanati [95]	LSDA + U	PAW	(5.45, 5.45, 5.45)		221	
	PBE + U		(5.55, 5.55, 5.55)		192	
Thompson [96]	PW91 + U	PAW	(5.54, 5.54, 5.54)		188	2.8
Tian [97]	PBE + U	PAW	(5.55, 5.55, 5.55)	21.8	192	2.2
Dorado [82]	LSDA + U	PAW	(5.41, 5.41, 5.41)	24.8	222	2.3

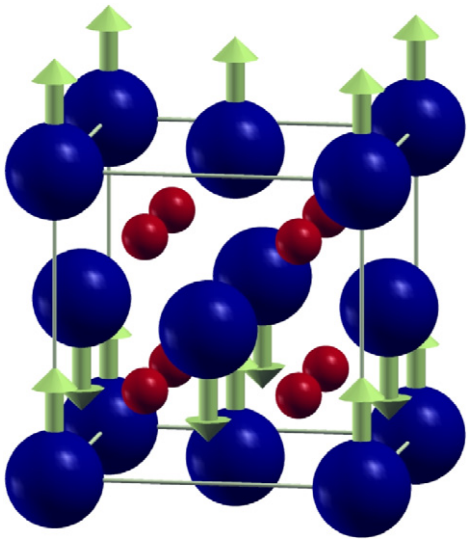

Figure 7. Fluorite structure of UO_2 with a collinear 1$\boldsymbol{k}$ antiferromagnetic order. Dark blue and red spheres stand for uranium and oxygen atoms, respectively. The arrows represent the directions of the uranium atomic magnetic moments.

formalism that can account for fluctuations between states, such as the DFT + DMFT.

Jollet *et al* [35] also used OMC together with EECE and confirmed the existence of metastable states within this formalism. They showed that breaking symmetries always yielded lower energy states and came up with a way to improve the initial wavefunctions (hence occupancies) of the calculations by using standard LDA/GGA. This method is at the basis of the U-ramping method described in section 3.2.

Geng *et al* [42] used the QA approach to find the ground state of 1$\boldsymbol{k}$ AFM UO_2. They first stated that the QA approach gave a solution lower in energy than the OMC, but it was later explained that the discrepancy was due to the PAW compensation charge rather than a failure of the OMC [83]. In addition, according to Geng *et al*, the QA approach breaks the symmetry of the crystal lattice. It therefore prevents all comparison with the calculations of Dorado *et al* [36] relative to the fluorite structure that were performed with symmetries.

Meredig *et al* [43] used the U-ramping method on a number of correlated materials including 1$\boldsymbol{k}$ AFM UO_2. They compared the results obtained with U-ramping and OMC, with and without symmetries. In both cases, the U-ramping yielded a total energy that is slightly higher than the OMC. In calculations without symmetries, Meredig *et al* reported that the lowest state obtained with U-ramping was located 5 meV/atom above the state obtained with OMC.

5.1.2. Ground state properties of UO_2. Basic properties of fluorite 1$\boldsymbol{k}$ AFM UO_2 (cell parameters, bulk modulus, bandgap and cohesive energy) have been extensively calculated using the DFT + U approximation, hybrid functionals and SIC. Results from these studies are all shown in table 2.

Cell parameters calculated in LDA + U and GGA + U are approximately 5.46 and 5.57 Å, respectively. Cohesive energies are in good agreement with the experimental value of 21.9 eV. Note that metastable states do not have a significant influence on these parameters, except for the bandgap value which can be affected by up to 20% [34, 35]. For the bulk modulus the scatter is larger than other properties (173 to 222 GPa) because the calculated value is strongly dependent

Table 3. Formation energies of neutral point defects in fluorite UO_2 calculated with DFT + U and EECE.

Authors	I_O	I_U	V_O	V_U	FP_O	FP_U	ISD
Iwasawa [87]	−0.4	4.7	4.5	8.4	4.1	13.1	
Gupta [88]	−1.6	8.2	5.6	6.0	4.0	14.2	7.2
Nerikar [90]	−1.3	6.1	5.3	9.0	4.0	15.1	7.6
Yu [92]	−2.4	2.5	5.1	4.5	2.6	7.0	3.6
Tiwary [105]					3.9	10.1	7.4
Dorado[a] [106]	−0.1	10.4	5.4	10.4	5.3	15.8	10.7
Andersson[a] [107]					5.3		10.2
Crocombette[a] [108]					6.4		9.9
Hong [109]			4.9	9.7			

[a] Done using occupation matrix control.

on the basis used, as well as on the way the energy–volume curve is fitted to the Murnaghan equation [98].

The thermal properties of UO_2 have been computed using DFT + U and DFT + DMFT via the determination of the phonon spectrum [94, 95, 99]. Using DFT + DMFT, Yin and Savrasov [99] computed the phonon spectrum of PM UO_2 and found it to be close to the experimental one [100], with an overall mismatch of approximately 15%. In addition, their calculated thermal conductivity was twice as low as the experimental value at 1000 K. Despite this they found that the only efficient heat carriers in UO_2 are the longitudinal acoustic phonons, which explains why UO_2 has such a low thermal conductivity. Devey [94] later used the OMC to reach the ground state of 1$\boldsymbol{k}$ AFM UO_2 and calculated the phonon frequencies in a 12-atom unit cell. The results are in good agreement with the experimental values, though less accurate than the DFT + DMFT calculations of Yin *et al*. Sanati *et al* [95] calculated several thermal properties of 1$\boldsymbol{k}$ AFM UO_2, including a Debye temperature of approximately 400 K, which compares well to the experimental values of 385 K [51] and 395 K [100].

Unlike fluorite 1$\boldsymbol{k}$ AFM UO_2, the low temperature phase (Jahn–Teller with 3$\boldsymbol{k}$ AFM order) has not been the subject of numerous studies. It was first studied by Laskowski *et al* [101] and the biggest difficulty is to model the 3$\boldsymbol{k}$ type AFM order. With spin–orbit coupling (SOC), Laskowski calculated the displacement of oxygen ions to be 0.16 Å with respect to the fluorite structure, which is significantly larger than the experimental estimate of 0.014 Å. The 3$\boldsymbol{k}$ AFM order, however, was not found to be the most stable magnetic ordering, in contradiction with experiments. Using OMC and without SOC, Dorado *et al* [36] calculated an oxygen displacement of 0.09 Å, with the 1$\boldsymbol{k}$ AFM order more stable than the 3$\boldsymbol{k}$ order. The greater stability of the 3$\boldsymbol{k}$ AFM order was first obtained by Gryaznov *et al* [102] using DFT + U, then by Zhou and Ozoliņš [103] with the self-interaction free DFT + U approximation.

It should be stressed that DFT + U, as a static mean field theory, can at most address the zero temperature limit, and it is therefore consistent to find as the most stable phase the 3$\boldsymbol{k}$ AFM structure of UO_2 with the JT distortion. Indeed, while the PM state can be described with DFT + U, it is still metastable compared to the JT phase [82]. At high temperature, the greater stability of the PM phase might for instance be studied with DFT + DMFT.

5.2. *Point defect properties*

5.2.1. Influence of spin–orbit coupling. Spin–orbit coupling (SOC) has been neglected in all DFT-based studies related to point defect behaviour in UO_2. While it appears a crude approximation given the heavy character of the uranium ion, it should not induce too great an error in the calculation of point defect formation energies and migration barriers.

Including SOC would result in two opposite effects: firstly the degeneracies would be lifted, hence an increase in the number of metastable states. Secondly the difference in energy between the $5f_{5/2}$ and $5f_{7/2}$ states is somewhat large and only the 5/2 states would be occupied. Since there are only six 5/2 states compared to 14 available without SOC, the number of metastable states should be lowered. We can expect, however, that the second effect is more important because of the large energy difference between the 5/2 and 7/2 states.

In addition, the Hubbard correction is still much larger than the SOC [104]. As a result, SOC has been neglected as a first step and it is expected to have an important impact on properties like crystal field levels and phonons, as well as properties derived from higher order derivatives of the total energy. For the study of nuclear fuel behaviour under irradiation, i.e. the calculation of point defect formation and activation energies, the effect of SOC is implicitly assumed by authors to be too small to strongly influence these physical quantities.

5.2.2. Formation energies. Point defect formation energies in fluorite UO_2 have long been a matter of debate because of the numerous discrepancies between results published in the literature. Table 3 shows the values calculated in 1$\boldsymbol{k}$ AFM UO_2 with DFT + U and EECE by various authors for the oxygen and uranium interstitial (I_O and I_U), the oxygen and uranium vacancy (V_O and V_U), the oxygen and uranium Frenkel pairs (FP_O and FP_U) and the isolated Schottky defect (ISD). In the ISD, the three vacancies do not interact, i.e. they are located far from one another. Note that the formation energies in table 3 correspond to that of neutral defects and can be expressed as

- Interstitial defects I_O and I_U: $E^F_{I_X} = E^{N+1}_{I_X} - E^N_{UO_2} - E_{ref}$.
- Vacancy defects V_O and V_U: $E^F_{V_X} = E^{N-1}_{V_X} - E^N_{UO_2} + E_{ref}$.

- Isolated Schottky defects ISD: $E^{\mathrm{F}}_{\mathrm{ISD}} = E^{N-1}_{\mathrm{V_U}} + 2 \times E^{N-1}_{\mathrm{V_O}} - 3 \times \frac{N-1}{N} \times E^{\mathrm{N}}_{\mathrm{UO_2}}$.
- Frenkel pairs: $E^{\mathrm{F}}_{\mathrm{FP_X}} = E^{N-1}_{\mathrm{V_X}} + E^{N+1}_{\mathrm{I_X}}$.

In the above equations, $E^{N+1}_{\mathrm{I_X}}$ is the total energy of a $(N+1)$-atom UO_2 supercell with an interstitial defect of type X (X = U, O), $E^{N-1}_{\mathrm{V_X}}$ is the total energy of a $(N-1)$-atom supercell with a vacancy defect of type X, $E^{\mathrm{N}}_{\mathrm{UO_2}}$ is the total energy of a N-atom supercell of perfect UO_2, and E_{ref} is the total energy of an arbitrary reference, such as the dioxygen molecule, the oxygen atom, metallic uranium in its α phase, the uranium atom, bulk UO_2, etc.

Looking at table 3, the discrepancies in the formation energies are striking. Should anyone need such formation energies, it would be impossible to decide which one is best, or even give an approximate value. It is difficult to compare the formation energies of defects that require reference states for oxygen and uranium (such as $\mathrm{I_O}$, $\mathrm{I_U}$, $\mathrm{V_O}$ and $\mathrm{V_U}$), because these reference states are arbitrary and can be calculated in several different ways (e.g. with DFT or DFT + U, with or without corrections, etc). This is why we rather compare the formation energies of defects that do not require such reference states, such as $\mathrm{FP_O}$, $\mathrm{FP_U}$ and ISD. We see that the formation energies range from 4.0 to 6.4 eV for the oxygen FP, from 7.0 to 15.8 eV for the uranium FP and from 3.6 to 10.7 eV for the ISD. This scatter is not acceptable for electronic structure calculations using similar approximations and parameters, which should display a better agreement.

It was shown that these discrepancies stem from the presence of metastable states in UO_2 [36]: in all studies in which no control has been done on electronic occupancies, the calculation of the perfect crystal always reached the first metastable state, located 12 meV/UO_2 above the ground state. The resulting error becomes significant for a 96-atom supercell and formation energies are therefore largely underestimated. It is argued in many DFT + U studies that this error cancels out in the calculation of the defective supercell. It is probably wrong. Indeed, if it cancelled out, all studies would find similar formation energies, which is not the case. In addition, we can see from table 3 that calculations using a proper treatment of metastable states (here, the OMC scheme, both with DFT + U and EECE) yield results that are in much better agreement, except for the $\mathrm{FP_O}$ formation energy calculated by Crocombette, which is slightly higher than that of Andersson and Dorado.

The reason why the error is not cancelled out is because there is no control of electronic occupancies. Therefore, the calculation of the defective supercell yields occupancies that are not those of the perfect crystal, even for atoms located far from the defect. As a result, the total energy difference between the defective and the perfect UO_2 supercells (hence the defect formation energy) is not consistent. When one uses the OMC scheme, the electronic occupancies of the perfect crystal are imposed on uranium atoms that are located far from the defect, so that their contribution is cancelled out in the total energy difference. Around the defects, the breaking of symmetries allows for an improved optimization of occupancies.

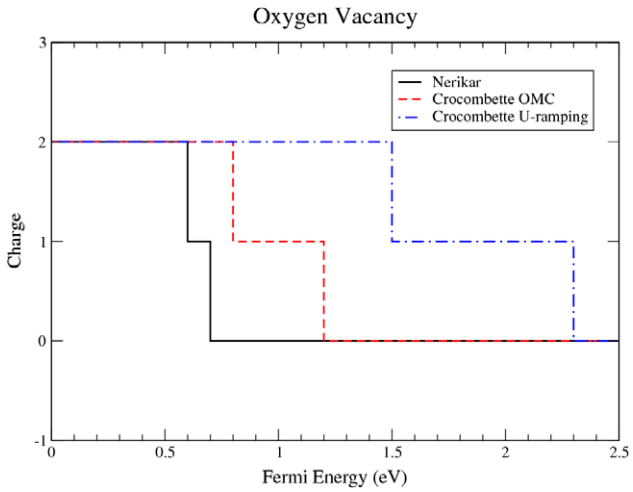

Figure 8. Range of stability of the charged oxygen vacancy with respect to the position of the Fermi level.

Charged defects in 1$\boldsymbol{k}$ AFM UO_2 have also been studied as follows:

- By Nerikar using DFT + U and no metastable state control method [90].
- By Andersson using DFT + U and OMC [107].
- By Crocombette using EECE and OMC [108].
- By Crocombette using DFT + U and U-ramping [110].

The oxygen vacancy (figure 8) is predicted to be charged +2 when the Fermi energy is close to the top of the valence band, i.e. when the material is hyper-stoichiometric. According to Nerikar, the most stable charge changes to +1 when the Fermi level is between 0.6 and 0.7 eV, and is neutral above this. Crocombette later used EECE + OMC and confirmed the stability of the +1 charge, but over a wider Fermi energy range, i.e. between 0.8 and 1.2 eV. Using U-ramping, however, Crocombette suggested that the +1 charge may be stable between 1.5 and 2.3 eV. Above 2.3 eV, the oxygen vacancy is neutral.

For the oxygen interstitial (figure 9), results differ again. Nerikar found the most stable charge to be −2 over the whole range of Fermi energies. On the contrary, Crocombette found with EECE + OMC that the charge would be 0 with a Fermi level between 0 and 0.3 eV, and −2 above. With U-ramping, another domain of stability is found, with a −1 charge between 0.3 and 0.8 eV.

As for the uranium vacancy (figure 10), it is predicted to be charged −4 over the whole range of Fermi energies by Nerikar and the first study by Crocombette using EECE + OMC. Using U-ramping, however, the uranium vacancy goes through all possible charge states from −4 to −1, over the whole range of Fermi energies.

While the above results certainly point out the importance of charge states for defects in UO_2, their stability range with respect to the Fermi energy is unclear. As with neutral defects, the discrepancies probably stem from the occurrence of metastable states. In order to assess more accurate ranges of stability for the charged defects in UO_2, additional

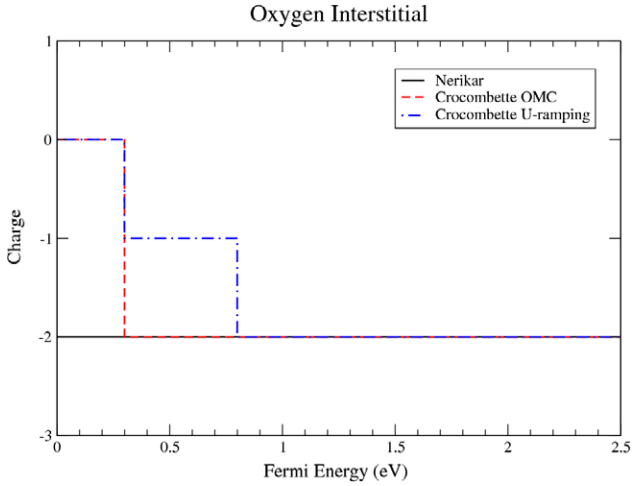

Figure 9. Range of stability of the charged oxygen interstitial with respect to the position of the Fermi level.

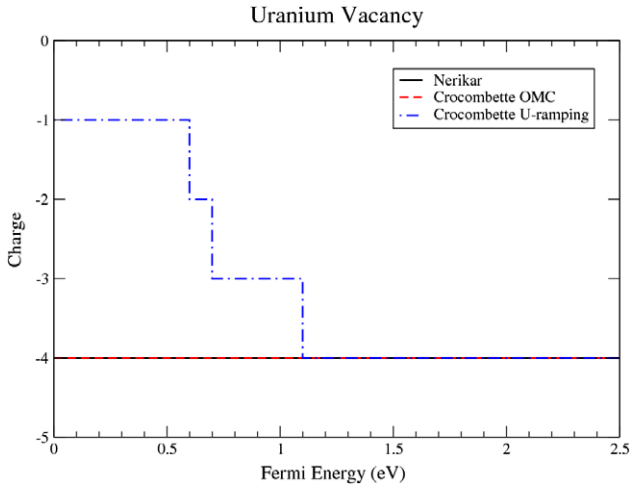

Figure 10. Range of stability of the charged uranium vacancy with respect to the position of the Fermi level.

calculations are therefore needed where metastable states are carefully controlled.

5.2.3. Activation energies for self-diffusion. There are very few DFT-based studies related to oxygen and uranium self-diffusion that employ approximations beyond DFT. For oxygen self-diffusion, the most favourable migration mechanism was found to be an indirect interstitial mechanism, in which an oxygen atom located on an interstitial site kicks an oxygen atom located on a lattice site, which in turn moves to the closest interstitial site. For this mechanism, Gupta *et al* [111] first calculated a migration barrier of −1.13 eV. As they found a negative migration energy, they suggested that the migration mechanism was occurring the other way round, i.e. both oxygen atoms start as a dumbbell and end up as one oxygen atom on a lattice site and the other on an interstitial site. Later, Dorado *et al* [75] suggested that this negative migration energy stemmed from the occurrence of metastable states, especially in the initial and final states of

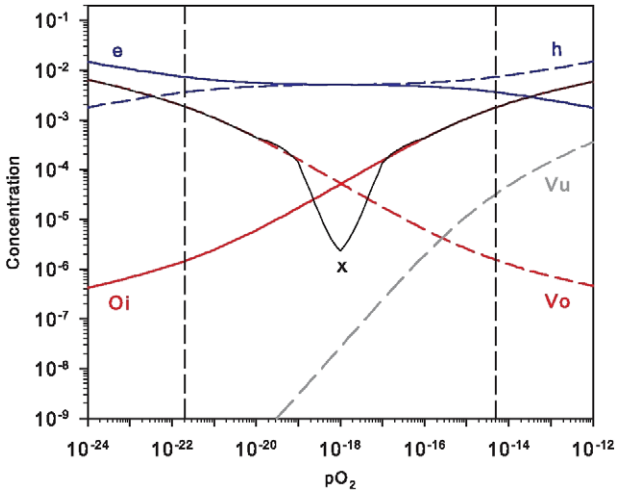

Figure 11. Changes as a function of oxygen potential of various defect concentrations and deviation from stoichiometry x, at 1600 K, calculated with DFT + U. The vertical dashed lines represent the domain of validity of the point defect model.

the migration path. They came up with a value of 0.93 eV for the same mechanism, using OMC. The resulting activation energy was first evaluated at 0.88 eV, but was later corrected to 0.63 eV [112] to account for the charged state of point defects in UO_2. The latter value compares very favourably with the latest experimental value of 0.75 ± 0.08 eV that was estimated from experiments carried out under controlled conditions [75].

As for uranium, the most favourable mechanism was found to be a vacancy mechanism along the ⟨110⟩ direction that involves a significant contribution from the oxygen sublattice, with a migration barrier of 3.6 eV [112]. Given the failure of previous point defect models [5, 7, 97, 108] to describe essential features of hyper-stoichiometric UO_{2+x}, in particular their tendency to predict more stable uranium vacancies, a new model has been developed that correctly reproduces the predominance of oxygen interstitials in the UO_{2+x} domain [112]. Figure 11 shows the corresponding Brouwer diagram, i.e. the changes as a function of oxygen potential of the various defect concentrations (electrons e, holes h, oxygen vacancies V_O, oxygen interstitials I_O and uranium vacancies V_U), as well as the deviation from stoichiometry x, at 1600 K. This study also pointed out the lack of accurate diffusion experiments carried out under controlled conditions.

6. Conclusion and outlook

While the issue of the metastable state has been known since the early developments of the Hartree–Fock theory, its importance in first-principles modelling of solid correlated systems was until recently largely overlooked. Actinide oxides are typically the kind of systems where the occurrence of metastable states has a significant influence, in particular in the calculation of formation, migration and activation energies. Bulk properties are essentially not affected, provided

one does not reach too high a metastable state. Among the three methods currently developed to avoid metastable states, the OMC is the most accurate one for determining the ground state of systems without point defects. This is due to the systematic character of the method, as well as its direct control over occupation matrices. When point defects are considered, however, the OMC scheme may become difficult to use. The *U*-ramping and QA approaches then appear as interesting alternatives.

Using these methods, point defect formation and migration energies have been calculated with more and more accuracy up to a precision that allows direct comparison with experiments, in particular related to atomic transport mechanisms, as evidenced by the few DFT-based studies on oxygen and uranium self-diffusion. All these studies have also pointed out the significant influence of electron correlations on the calculated formation energies and migration barriers, which enabled the experimental data to be reproduced. There is still, however, a lot to accomplish on UO_2. Recent studies have pointed out the importance of charged states for point defects and the range of stability of charged states with respect to the Fermi level currently shows significant discrepancies. On another level, UO_2 doping, clustering of defects and fission product migration are now being extensively studied with DFT as the next step in the understanding of the fuel behaviour under irradiation. The complexity of these calculations, especially related to their time and length scales, now requires DFT to be coupled to other methods such as quantum and classical molecular dynamics, kinetic Monte Carlo, etc. With the constant development of new approaches and increase in computational power, however, there is no doubt that the next decade will see a significant amount of work related to these phenomena, possibly up to a complete multiscale picture of the behaviour of UO_2 under irradiation.

Acknowledgments

The following people are gratefully acknowledged for discussions and collaborations on related studies: David A Andersson, François Bottin, Jean-Paul Crocombette, François Jollet, Guillaume Martin, Christopher R Stanek, Gabriel Stoltz, Marc Torrent, Doru Torumba, Blas P Uberuaga and Emerson Vathonne.

References

[1] Hohenberg P and Kohn W 1964 Inhomogeneous electron gas *Phys. Rev.* **136** 864
[2] Kohn W and Sham L J 1965 Self-consistent equations including exchange and correlation effects *Phys. Rev.* **140** 1133
[3] Petit T, Lemaignan C, Jollet F, Bigot B and Pasturel A 1998 Point defects in uranium dioxide *Phil. Mag.* B **77** 779
[4] Petit T, Jomard G, Lemaignan C, Bigot B and Pasturel A 1999 Location of krypton atoms in uranium dioxide *J. Nucl. Mater.* **275** 119
[5] Crocombette J-P, Jollet F, Thien Nga L and Petit T 2001 Plane-wave pseudopotential study of point defects in uranium dioxide *Phys. Rev.* B **64** 104107
[6] Crocombette J-P 2002 *Ab initio* energetics of some fission products (Kr, I, Cs, Sr and He) in uranium dioxide *J. Nucl. Mater.* **305** 29
[7] Freyss M, Petit T and Crocombette J-P 2005 Point defects in uranium dioxide: *ab initio* pseudopotential approach in the generalized gradient approximation *J. Nucl. Mater.* **347** 347
[8] Freyss M, Vergnet N and Petit T 2006 *Ab initio* modeling of the behavior of helium and xenon in actinide dioxide nuclear fuels *J. Nucl. Mater.* **352** 144
[9] Liu X-Y, Andersson D A and Uberuaga B P 2012 First-principles DFT modeling of nuclear fuel materials *J. Mater. Sci.* **47** 7367
[10] Adamo C and Barone V 1999 Toward reliable density functional methods without adjustable parameters: the PBE0 model *J. Chem. Phys.* **110** 6158
[11] Heyd J, Scuseria G E and Ernzerhof M 2003 Hybrid functionals based on a screened coulomb potential *J. Chem. Phys.* **118** 8207
[12] Prodan I D, Scuseria G E and Martin R L 2007 Covalency in the actinide dioxides: systematic study of the electronic properties using screened hybrid density functional theory *Phys. Rev.* B **76** 033101
[13] Petit L, Svane A, Szotek Z and Temmerman W 2003 First-principles calculations on $PuO_{2\pm x}$ *Science* **301** 498
[14] Anisimov V I, Zaanen J and Andersen O K 1991 Band theory and Mott insulators: Hubbard U instead of stoner I *Phys. Rev.* B **44** 943
[15] Liechtenstein A I, Anisimov V I and Zaanen J 1995 Density-functional theory and strong interactions: orbital ordering in Mott–Hubbard insulators *Phys. Rev.* B **52** R5467
[16] Dudarev S L, Botton G A, Savrasov S Y, Humphreys C J and Sutton A P 1998 Electron-energy-loss spectra and the structural stability of nickel oxide: an LSDA + *U* study *Phys. Rev.* B **57** 1505
[17] Georges A, Kotliar G, Krauth W and Rozenberg M J 1996 Dynamical mean-field theory of strongly correlated fermion systems and the limit of infinite dimensions *Rev. Mod. Phys.* **68** 13
[18] Kotliar G, Savrasov S Y, Haule K, Oudovenko V S, Parcollet O and Marianetti C A 2006 Electronic structure calculations with dynamical mean-field theory *Rev. Mod. Phys.* **78** 865
[19] Novák P, Kunes J, Chaput L and Pickett W E 2006 Exact exchange for correlated electrons *Phys. Status Solidi* b **243** 563
[20] Ylvisaker E R, Pickett W E and Koepernik K 2009 Anisotropy and magnetism in the LSDA + *U* method *Phys. Rev.* B **79** 035103
[21] Czyżyk M T and Sawatzky G A 1994 Local-density functional and on-site correlations: the electronic structure of La_2CuO_4 and $LaCuO_3$ *Phys. Rev.* B **49** 14211
[22] Zhou F and Ozoliņš V 2009 Obtaining correct orbital ground states in f-electron systems using a nonspherical self-interaction-corrected lda+u method *Phys. Rev.* B **80** 125127
[23] Gunnarsson O, Andersen O K, Jepsen O and Zaanen J 1989 Density-functional calculation of the parameters in the anderson model: application to mn in cdte *Phys. Rev.* B **39** 1708
[24] Cococcioni M and de Gironcoli S 2005 Linear response approach to the calculation of the effective interaction parameters in the LDA + *U* method *Phys. Rev.* B **71** 035105
[25] Aryasetiawan F, Imada M, Georges A, Kotliar G, Biermann S and Lichtenstein A I 2004 Frequence-dependent local interactions and low-energy effective models from electornic structure calculations *Phys. Rev.* B **70** 195104

[26] Karlsson K, Aryasetiawan F and Jepsen O 2010 Method for calculating the electronic structure of correlated materials from a truly first-principles LDA + U scheme *Phys. Rev.* B **81** 245113

[27] Yamazaki T and Kotani A 1991 Systematic analysis of 4f core photoemission spectra in actinide oxides *J. Phys. Soc. Japan* **60** 49

[28] Kotani A and Yamazaki T 1992 Systematic analysis of core photoemission spectra for actinide di-oxides and rare-earth sesqui-oxides *Prog. Theor. Phys. Suppl.* **108** 117

[29] Yin Q, Kutepov A, Haule K, Kotliar G, Savrasov S Y and Pickett W E 2011 Electronic correlation and transport properties of nuclear fuel materials *Phys. Rev.* B **84** 195111

[30] Shick A B, Pickett W E and Liechtenstein A I 2001 Ground and metastable states in γ-ce from correlated band theory *J. Electron Spectrosc. Relat. Phenom.* **114–116** 753

[31] Kudin K N, Scuseria G E and Martin R L 2002 Hybrid density-functional theory and the insulating gap of UO_2 *Phys. Rev. Lett.* **89** 266402

[32] Prodan I D, Scuseria G E and Martin R L 2006 Assessment of metageneralized gradient approximation and screened coulomb hybrid density functionals on bulk actinide oxides *Phys. Rev.* B **73** 045104

[33] Larson P, Lambrecht W R L, Chantis A N and van Schilfgaarde M 2007 Electronic structure of rare-earth nitrides using the LDA + U approach: importance of allowing 4f orbitals to break the cubic crystal symmetry *Phys. Rev.* B **75** 045114

[34] Dorado B, Amadon B, Freyss M and Bertolus M 2009 DFT + U calculations of the ground state and metastable states of uranium dioxide *Phys. Rev.* B **79** 235125

[35] Jollet F, Jomard G, Amadon B, Crocombette J-P and Torumba D 2009 Hybrid functional for correlated electrons in the projector augmented-wave formalism: study of multiple minima for actinide oxides *Phys. Rev.* B **80** 235109

[36] Dorado B, Jomard G, Freyss M and Bertolus M 2010 Stability of oxygen point defects in UO_2 by first-principles DFT + U calculations: occupation matrix control and Jahn–Teller distortion *Phys. Rev.* B **82** 035114

[37] Amadon B 2012 A self-consistent DFT + DMFT scheme in the projector augmented wave method: applications to cerium, Ce_2O_3 and Pu_2O_3 with the Hubbard i solver and comparison to DFT + U *J. Phys.: Condens. Matter* **24** 075604

[38] Adams W H 1962 Stability of the Hartree–Fock states *Phys. Rev.* **127** 1650

[39] Fukutome H 1981 Unrestricted Hatree–Fock theory and its applications to molecules and chemical reactions *Int. J. Quantum Chem.* **20** 965

[40] Amadon B, Jollet F and Torrent M 2008 Gamma and beta cerium: LDA + U calculations of ground-state parameters *Phys. Rev.* B **77** 155104

[41] Jomard G, Amadon B, Bottin F and Torrent M 2008 Structural, thermodynamic, and electronic properties of plutonium oxides from first principles *Phys. Rev.* B **78** 075125

[42] Geng H Y, Chen Y, Kaneta Y, Kinoshita M and Wu Q 2010 Interplay of defect cluster and the stability of xenon in uranium dioxide from density functional calculations *Phys. Rev.* B **82** 094106

[43] Meredig B, Thompson A, Hansen H A, Wolverton C and van de Walle A 2010 Method for locating low-energy solutions within DFT + U *Phys. Rev.* B **82** 195128

[44] Thom A J W and Head-Gordon M 2008 Locating multiple self-consistent field solutions: an approach inspired by metadynamics *Phys. Rev. Lett.* **101** 193001

[45] Pourovskii L V, Delaney K T, Van de Walle C G, Spaldin N A and Georges A 2009 Role of atomic multiplets in the electronic structure of rare-earth semiconductors and semimetals *Phys. Rev. Lett.* **102** 096401

[46] Willis B T M 1963 Neutron diffraction studies of the actinides oxides. I. Uranium dioxide and thorium dioxide at room temperature *Proc. R. Soc.* A **274** 122

[47] Idiri M, Le Bihan T, Heathman S and Rebizant J 2004 Behavior of actinide dioxides under pressure: UO_2 and ThO_2 *Phys. Rev.* B **70** 014113

[48] Brandt O G and Walker C T 1967 Temperature dependence of elastic constants and thermal expansion for UO_2 *Phys. Rev. Lett.* **18** 11

[49] Wachtman J B, Wheat M L, Anderson H J and Bates J L 1965 Elastic constants of single crystal UO_2 at 25 °C *J. Nucl. Mater.* **16** 39

[50] Marlowe M O 1969 High temperature isothermal elastic moduli of UO_2 *J. Nucl. Mater.* **33** 242

[51] Fritz I J 1976 Elastic properties of UO_2 at high pressure *J. Appl. Phys.* **47** 4353

[52] Benedict U, Andreetti G D, Fournier J M and Waintal A 1982 X-ray powder diffraction study of the high pressure behaviour of uranium dioxide *J. Physique Lett.* **43** 171

[53] Baer Y and Schoenes J 1980 Electronic structure and coulomb correlation energy in UO_2 single crystal *Solid State Commun.* **33** 885

[54] Schoenes J 1978 Optical properties and electronic structure of UO_2 *J. Appl. Phys.* **49** 1463

[55] Killeen J C 1980 The effect of niobium oxide additions on the electrical conductivity of UO_2 *J. Nucl. Mater.* **88** 185

[56] Kelly P J and Brooks M S S 1987 Electronic structure and ground state properties of the actinide oxides *J. Chem. Soc. Faraday Trans.* 2 **83** 1189

[57] Lander G H, Faber J, Freeman A J and Desclaux J P 1976 Neutron-diffraction study of UO_2: paramagnetic state *Phys. Rev.* B **13** 1177

[58] Santini P, Carretta S, Amoretti G, Caciuffo R, Magnani N and Lander G H 2009 Multipolar interactions in f-electron systems: the paradigm of actinide dioxides *Rev. Mod. Phys.* **81** 807

[59] Caciuffo R, Amoretti G, Santini P, Lander G H, Kulda J and Du Plessis P de V 1999 Magnetic excitations and dynamical Jahn–Teller distortions in UO_2 *Phys. Rev.* B **59** 13892

[60] Jones W M, Gordon J and Long E A 1952 The heat capacities of uranium, uranium trioxide, and uranium dioxide from 15 K to 300 K *J. Chem. Phys.* **20** 695

[61] Arrott A and Goldman J E 1957 Magnetic analysis of the uranium-oxygen system *Phys. Rev.* **108** 948

[62] Frazer B C, Shirane G and Cox D E 1965 Neutron-diffraction study of antiferromagnetism in UO_2 *Phys. Rev.* **140** 1448

[63] Faber J and Lander G H 1976 Neutron diffraction study of UO_2: antiferromagnetic state *Phys. Rev.* B **14** 1151

[64] Allen S J 1968 Spin-lattice interaction in UO_2. I. Ground-state and spin-wave excitations *Phys. Rev.* **166** 530

[65] Allen S J 1968 Spin-lattice interaction in UO_2. II. Theory of the first-order phase transition *Phys. Rev.* **167** 492

[66] Faber J, Lander G H and Cooper B R 1975 Neutron-diffraction study of UO_2: observation of an internal distortion *Phys. Rev. Lett.* **35** 1770

[67] Burlet P, Rossat-Mignod J, Vuevel S, Vogt O, Spirlet J C and Rebizant J 1986 Neutron diffraction on actinides *J. Less-Common Met.* **121** 121

[68] Ikushima K, Tsutsui S, Haga Y, Yauoka H, Walstedt R E, Masaki N M, Nakamura A, Nasu S and Ōnuki Y 2001 First-order phase transition in UO_2: ^{235}U and ^{17}O NMR study *Phys. Rev.* B **63** 104404

[69] Blackburn E, Caciuffo R, Magnani N, Santini P, Brown P J, Enderle M and Lander G H 2005 Spherical neutron spin polarimetry of anisotropic magnetic fluctuations in UO_2 *Phys. Rev.* B **72** 184411

[70] Wilkins S B, Caciuffo R, Detlefs C, Rebizant J, Colineau E, Wastin F and Lander G H 2006 Direct observation of electric-quadrupolar order in UO_2 *Phys. Rev.* B **73** 060406

[71] Auskern A B and Belle J 1961 Oxygen ion self-diffusion in uranium dioxide *J. Nucl. Mater.* **3** 267

[72] Belle J 1969 Oxygen and uranium diffusion in uranium dioxide (a review) *J. Nucl. Mater.* **30** 3

[73] Marin J F and Contamin P 1969 Uranium and oxygen self-diffusion in UO_2 *J. Nucl. Mater.* **30** 16

[74] Murch G E and Catlow C R A 1987 Oxygen diffusion in UO_2, ThO_2 and PuO_2—a review *J. Chem. Soc. Faraday Trans.* 2 **83** 1157

[75] Dorado B *et al* 2011 First-principles calculation and experimental study of oxygen diffusion in uranium dioxide *Phys. Rev.* B **83** 035126

[76] Reimann D K and Lundy T S 1969 Diffusion of ^{233}U in UO_2 *J. Am. Ceram. Soc.* **52** 511

[77] Matzke H 1969 On uranium self-diffusion in UO_2 and UO_{2+x} *J. Nucl. Mater.* **30** 26

[78] Matzke H 1987 Atomic transport properties in UO_2 and mixed oxides (U, Pu)O_2 *J. Chem. Soc. Faraday Trans.* **83** 1121

[79] Sabioni A C S, Ferraz W B and Millot F 1998 First study of uranium self-diffusion in UO_2 by SIMS *J. Nucl. Mater.* **257** 180

[80] Garcia P, Fraczkiewicz M, Davoisne C, Carlot G, Pasquet B, Baldinozzi G, Simeone D and Petot C 2010 Oxygen diffusion in relation to p-type doping in uranium dioxide *J. Nucl. Mater.* **400** 112

[81] Sabioni A C S, Ferraz W B and Millot F 2000 Effect of grain-boundaries on uranium and oxygen diffusion in polycrystalline UO_2 *J. Nucl. Mater.* **278** 364

[82] Dorado B and Garcia P 2013 First-principles DFT + U modeling of actinide-based alloys: application to paramagnetic phases of UO_2 and (U, Pu) mixed oxides *Phys. Rev.* B **87** 195139

[83] Dorado B, Amadon B, Jomard G, Freyss M and Bertolus M 2011 Comment on 'interplay of defect cluster and the stability of xenon in uranium dioxide from density functional calculations' *Phys. Rev.* B **84** 096101

[84] Dudarev S L, Nguyen Mahn D and Sutton A P 1997 Effect of Mott–Hubbard correlations on the electronic structure and structural stability of uranium dioxide *Phil. Mag.* B **75** 613

[85] Dudarev S L, Botton G A, Savrasov S Y, Szotek Z, Temmerman W M and Sutton A P 1998 Electronic structure and elastic properties of strongly correlated metal oxides from first principles: LSDA + U, SIC-LSDA and EELS study of UO_2 and NiO *Phys. Status Solidi* a **166** 429

[86] Yun Y, Kim Ha, Kim He and Park K 2005 *Ab initio* calculations of strongly correlated electrons: antiferromagnetic ground state of UO_2 *Nucl. Eng. Technol.* **37** 293

[87] Iwasawa M, Chen Y, Kaneta Y, Ohnuma T, Geng H Y and Kinoshita M 2006 First-principles calculation of point defects in uranium dioxide *Mater. Trans.* **47** 2651

[88] Gupta F, Brillant G and Pasturel A 2007 Correlation effects and energetics of point defects in uranium dioxide: a first principle investigation *Phil. Mag.* **87** 2561

[89] Geng H Y, Chen Y, Kaneta Y and Kinoshita M 2007 Structural behavior of uranium dioxide under pressure by LSDA + U calculations *Phys. Rev.* B **75** 054111

[90] Nerikar P V, Watanabe T, Tulenko J S, Phillpot S R and Sinnott S B 2009 Energetics of intrinsic point defects in uranium dioxide from electronic-structure calculations *J. Nucl. Mater.* **384** 61

[91] Gryaznov D, Heifets E and Kotomin E 2009 *Ab initio* DFT + U study of he atom incorporation into UO_2 crystals *Phys. Chem. Chem. Phys.* **11** 7241

[92] Yu J, Devanathan R and Weber W J 2009 First-principles study of defects and phase transition in UO_2 *J. Phys.: Condens. Matter* **21** 435401

[93] Petit L, Svane A, Szotek Z, Temmerman W M and Stocks G M 2010 Electronic structure and ionicity of actinide oxides from first principles *Phys. Rev.* B **81** 045108

[94] Devey A J 2011 First principles calculation of the elastic constants and phonon modes of UO_2 using GGA + U with orbital occupancy control *J. Nucl. Mater.* **412** 301

[95] Sanati M, Albers R C, Lookman T and Saxena A 2011 Elastic constants, phonon density of states, and thermal properties of UO_2 *Phys. Rev.* B **84** 014116

[96] Thompson A E and Wolverton C 2011 First-principles study of noble gas impurities and defects in UO_2 *Phys. Rev.* B **84** 134111

[97] Tian X, Gao T, Jiang G, He D and Xiao H 2012 The incorporation and solution of krypton in uranium dioxide: density functional theory calculations *Comput. Mater. Sci.* **54** 188

[98] Birch F 1947 Finite elastic strain of cubic crystals *Phys. Rev.* **71** 809

[99] Yin Q and Savrasov S Y 2008 Origin of low thermal conductivity in nuclear fuels *Phys. Rev. Lett.* **100** 225504

[100] Dolling G, Cowley R A and Woods A D B 1965 The crystal dynamics of uranium dioxide *Can. J. Phys.* **43** 1397

[101] Laskowski R, Madsen G K H, Blaha P and Schwarz K 2004 Magnetic structure and electric-field gradients of uranium dioxide: an *ab initio* study *Phys. Rev.* B **69** 140408

[102] Gryaznov D, Rashkeev S, Kotomin E A, Heifets E and Zhukovskii Y 2010 Helium behavior in oxide nuclear fuels: first principles modeling *Nucl. Instrum. Methods* B **268** 3090

[103] Zhou F and Ozoliņš V 2011 Crystal field and magnetic structure of UO_2 *Phys. Rev.* B **83** 085106

[104] Santini P, Lémanski R and Erdös P 1999 Magnetism of actinide compounds *Adv. Phys.* **48** 537

[105] Tiwary P, van de Walle A and Grønbech-Jensen N 2009 *Ab initio* construction of interatomic potentials for uranium dioxide across all interatomic distances *Phys. Rev.* B **80** 174302

[106] Dorado B 2010 Electronic structure calculations of atomic transport properties in uranium dioxide: influence of strong correlations *PhD Thesis* University of Aix-Marseille II, France

[107] Andersson D A, Uberuaga B P, Nerikar P V, Unal C and Stanek C R 2011 U and Xe transport in $UO_{2\pm x}$: density functional theory calculations *Phys. Rev.* B **84** 054105

[108] Crocombette J-P, Torumba D and Chartier A 2011 Charge states of point defects in uranium oxide calculated with a local hybrid functional for correlated electrons *Phys. Rev.* B **83** 184107

[109] Hong M, Phillpot S R, Lee C-W, Nerikar P, Uberuaga B P, Stanek C R and Sinnot S B 2012 Solubility and clustering of ruthenium fission products in uranium dioxide as determined by density functional theory *Phys. Rev.* B **85** 144110

[110] Crocombette J-P 2012 Influence of charge states on energies of point defects and clusters in uranium dioxide *Phys. Rev.* B **85** 144101

[111] Gupta F, Pasturel A and Brillant G 2010 Diffusion of oxygen in uranium dioxide: a first-principles investigation *Phys. Rev.* B **81** 014110

[112] Dorado B, Andersson D A, Stanek C R, Bertolus M, Uberuaga B P, Martin G, Freyss M and Garcia P 2012 First-principles calculations of uranium diffusion in uranium dioxide *Phys. Rev.* B **86** 035110